Open Science

Geological, Multispectral and Aeromagnetic Expressions of Pegmatite Hosted Mineralization of Keffi Sheet 208 NE, North-Central Nigeria

Ejepu Jude Steven[1, *], Arikawe Eniafe Adepitan[2], Abdullahi Suleiman[1]

[1]Department of Geology, School of Physical Sciences, Federal University of Technology, Minna, Nigeria

[2]Prototype Engineering Development Institute (PEDI), National Agency for Science and Engineering Infrastructure (NASENI), Ilesha, Nigeria

Email address

ejepu.jude@futminna.edu.ng (E. J. Steven)

[*]Corresponding author

Abstract

An integrated spectral and structural interpretation of pegmatite hosted mineralization was carried out in sheet 208 NE in order to characterise specific spectral and geophysical features in an attempt to narrow down areas for further mineral exploration. The area is characterized by over eighty pegmatites exposures hosted by the gneiss, schist and igneous rock units. Landsat 8 Operational Land Imager (OLI), Shuttle Radar Topographic Mission Digital Elevation Model (SRTM DEM) and aeromagnetic datasets with acquired field geological information were used in this study. Data obtained from field structural mapping was used to produce a rose diagram to illustrate principal joint directions. Landsat 8 image was processed using band ratios for RGB colour composites for lineament extraction and target selection. SRTM DEM and aeromagnetic data were also processed to obtain derivative maps from which lineaments were also extracted. Lineaments from different datasets were integrated to form a composite lineament map of the area. Pegmatite bodies are more prominent in the schist. Geological boundaries and contact zones and a few shear zones have metal bearing pegmatites. Foliation planes (schist and gneiss) and fractures of granites are all rich with pegmatite veins and dykes. Rare-metal pegmatites are close to major and subsidiary fault structures. Structural analyses revealed a major NE-SW for the magnetic lineaments and NW-SE trend for the surface lineaments. Alteration zones marked by the presence of iron oxides, hydroxyl- bearing minerals and hydrothermal clays were delineated from a composite of different band ratios. The result of this study positively supports a more detailed exploration from selected alteration zones.

Keywords

Pegmatites, Mineral Exploration, Remote Sensing, Aeromagnetic Data, Lineaments

1. Introduction

Increasing industrialization associated with development of high-tech devices and the concomitant expanding demands of specialized raw materials, rare metals and rare earth elements (REE) are playing fundamental functions in this regard. This increasing demand necessitates exploration for potential rare metals and REE deposits. Also, this would support the efforts of the government in the diversification of the economy so as not to depend wholly on crude oil for foreign exchange.

Major occurrences of pegmatites are found around north-central to north-western part of the country. Ore mineral pegmatites containing economic concentrations of different rare metals are widespread in the Pan-African (600 ± 150Ma) basement of Nigeria. These pegmatites are also important

sources of precious and semi-precious stones (such as beryl, aquamarine, tourmalines). These pegmatites have been described as a broad 400 km long NE-SW trending belt, though recent publications have deciphered that these pegmatites are more widely distributed than previously known [1].

Some of the researches previously carried out in around the study area have reported a series of dykes and irregular pegmatite bodies usually forming prominent ridges [2-4]. Mineralisation is reported to be in the form of dissemination and discrete concentrations of columbite–tantalite accompanied by cassiterite, ilmenite, Fe-oxides and occasionally bismuthinite and fluorite.

Therefore, in this study, an attempt has been made to comprehensively integrate spectral and structural attributes extracted from Landsat 8 Operational Land Imager (OLI), Shuttle Radar Topographic Mission Digital Elevation Model (SRTM DEM) and aeromagnetic datasets with acquired field geological information to characterize specific spectral and geophysical features in order to narrow down target areas for further exploration in the area and other areas having similar deposits.

The study area is part of the Basement Complex of Nigeria, within which four major lithological units are distinguishable, namely:

1. The Migmatite – Gneiss Complex (M-Gc)

2. The Schist Belt (Meta-sedimentary and Meta-volcanic rocks)

3. The Older Granites (Pan African granitoids)

4. Un-deformed Acid and Basic Dykes [5]

These rocks all constitute the Pre-Cambrian to Lower Palaeozoic Basement Complex rocks. The gneiss-migmatites bears imprints of the Liberian (ca. 2500Ma), Eburnean (ca. 2000Ma) and Pan African (ca. 600Ma) tectonic events [6-7]. Within the sequence are domains of meta-sediments and meta-volcanics intruded by igneous rocks, which constitute the north/south trending schist belts. The schist belt lithologies which consist of fine grained clastics, pelitic schists, phyllites, banded iron-formations, marble and amphibolites are considered to be Upper Proterozoic assemblages [7]. They host most of the economic minerals in the Basement Complex. During the Pan-African episode, the Proterozoic migmatite-gneiss-schist complex were intruded by various granitoids resulting from oceanic closure, subduction, oblique collision between the West African Craton and the Hoggar – Nigeria shields [8] and crustal thickening. The Pan-African granitoids of Nigeria, which are collectively termed Older Granites, comprise gabbros, charnockites, diorites, granites, and syenites. Geo-chronological data from previous works (Rb–Sr whole-rock and U-Pb zircon) on Pan-African granitoids intruding the reactivated Archean to Lower Proterozoic crust of central and south-western Nigeria show that intrusive migmatite activity in these areas lasted from at least 630 to 530 Ma [9-14].

Results of the rock ages also show that pegmatite emplacement in the southwestern Nigeria occurred mainly after the peak of the Pan-African orogenic event in this area. The end of the Pan-African tectonic event is marked by a conjugate fracture system of the strike-slip faults [15]. Fault directions have consistent trend and sense of displacement; i.e. a NE-SW (NNE-SSW) trending system having a dextral sense of movement and a NW-SE trending system a sinistral sense [15-18]. Both sets crosscut all the main Pan-African structures, including older N-S trending shear zones (mylonites) and late orogenic granites [15, 19-21]. Gold and pegmatite rare earth mineralization are closely associated with the fractures in the Pan-African belt [20-23, 2]. About 100 km north-east of the area of study at Wamba, rare metal pegmatites have also been geochemically linked to pre-aluminous late Pan-African tectonic granitoids, the emplacement of which have largely been controlled by the regional fractures [20]. Chemical data on granites, and granitic and pegmatitic muscovites show that RB, Cs, Sn, Nb, and Ta are enriched during both magmatic and post-magmatic evolution, with the highest contents of these elements occurring in early muscovites of the albitized and mineralized pegmatites [20]. Albite, k-feldspar, and quartz are the main pegmatite-forming mineral; white mica is a typical but minor component.

2. Method

In mineral exploration studies, the selection of the most adequate methods is directly associated to the mode of formation and occurrence of the targeted mineral deposits [24]. Since this study targets pegmatites which occur in veins and dykes and/or related to shear zones, possible surface manifestations of these features are structural controlled and are usually expressed as lineaments.

Therefore, lineaments as adopted in this study are delineated on maps as rectilinear or slightly curvilinear features that are surface manifestations of geological phenomena occurring within the earth [25]. Lineaments account for geological structures that include faults, shear zones, joint patterns and intrusives. However, other features not having direct geological significance may mimic these features. These may include aligned water courses and valleys, topographical alignments and vegetation contrasts. Effort has been made to remove these from interpretations made in this research.

Spaceborne remote sensing techniques have been extensively used to explore for natural resources on earth's surface. Each mineral or rock may have its own unique spectral pattern of scattering and absorption features known as its spectral signature. This spectral signature is often used to identify a target mineral remotely. Hydrothermal alteration and iron oxides are reported to occur in Keffi Sheet 208 [4], therefore, band rationing can help to emphasize spectral contrast and to map the iron mineral's distribution [26-28].

Iron oxides and oxide-hydroxides are among the most common minerals in nature. Common iron oxide minerals include hematite (Fe_2O_3), goethite (FeOOH), and magnetite (Fe_3O_4). Iron minerals often present in altered

rocks can produce unique spectral features, including hematite, goethite, magnetite, and jarosite. Spectral information of hydrothermally altered rocks and minerals is very useful due to their mineralogical association with valuable deposits. Spectral signatures displayed in the visible and near infrared spectrum (0.35 to 1.0 µm) are caused by iron cations through electronic processes of crystal-effects and charge-transfer absorptions [29], whereas spectral signatures at wavelengths longer than 1.0 µm but less than 2.5 µm are caused by the vibrational transitions of hydroxyl-bearing minerals [30]

An aeromagnetic anomaly is caused by lateral variations of Earth's materials that can be considered as a vector sum (total magnetization) of induced and remnant magnetization [31]. Igneous intrusions often correspond to high magnetic anomalies compared to country rocks.

2.1. Materials

2.1.1. SRTM DEM

SRTM was launched on February 11, 2000 as an international project spearheaded by the National Imagery and Mapping Agency (NIMA) and National Aeronautics and Space Administration (NASA) in cooperation with the German Aerospace Centre (DLR). The main objective of the SRTM mission is to obtain elevation data on a near-global scale and generate the most complete high-resolution digital topographic database of the Earth. Using the Space borne Imaging Radar-C and X-Band Synthetic Aperture Radar (SIR-C and X-SAR) hardware, SRTM collects data that are used to generate a digital elevation model with data points spaced every 1 arc second of latitude and longitude (approximately 30 metres at the equator). The absolute horizontal and vertical accuracy is better than 20 metres and 16 metres, respectively. SRTM uses radar interferometry. The 30 m SRTM data was downloaded from [32]. This site is an interface that attempts to ease the pain of downloading 30-meter resolution elevation data from the Shuttle Radar Topography Mission website.

2.1.2. Landsat 8 OLI

This is the latest instrument in the Landsat series of satellite imagers, launched aboard the Landsat-8 in February 2013. The OLI continues the legacy of Landsat, building the archive of moderate resolution earth imagery, but the instrument itself is significantly different than the Thematic Mapper (TM) series of sensors aboard Landsat-5 and -7. The TM instruments were whiskbroom sensors with relatively few detectors sweeping over the earth in the cross-track direction of the satellite. The OLI is a pushbroom sensor, with long arrays of detectors forming the image as the satellite moves across the Earth. Unlike the TMs, OLI does not include a thermal band. The Thermal Infrared Sensor (TIRS) covers the thermal region and has two bands [33]. Table 1 shows the spectral band characteristics OLI and TIRS.

Table 1. Landsat 8 band specifications Source: USGS/NASA [34].

Sensor	Band	Spectral Resolution (µm)	Spatial resolution (m)
OLI	Band 1 - Coastal	0.435-0.451	30
	Band 2 - Blue	0.452-0.512	30
	Band 3 - Green	0.533-0.590	30
	Band 4 - Red	0.636-0.673	30
	Band 5 - NIR	0.851-0.879	30
	Band 6 - SWIR-1	1.566-1.651	30
	Band 7 - SWIR-2	2.107-2.294	30
	Band 8 - Pan	0.503-0.676	15
	Band 9 - Cirrus	1.363-1.384	30
TIRS	Band 10 - TIR-1	10.6-11.19	100
	Band 11 - TIR-2	11.50-12.51	100

The Landsat 8 used in this research available from [35] was clipped from scene path 189 row 054 LC08_L1TP_189054_20160315_20170328_01_T1 from 15th March, 2016. This scene was chosen due to its virtually non-existent cloud cover of about 1% and perfect image quality of 100%.

2.1.3. Aeromagnetic Data

The aeromagnetic inversion method is based on processing of the total field magnetic anomaly. Total magnetization is the rock property associated to its magnetic anomaly and geologic origin [36] in the direction of the earth's field. The total field aeromagnetic anomalies include both induced and remnant magnetic fields. This is a reflection of variations in the amount and type of subsurface magnetic minerals, hence, important for geophysical prospecting of mineral resources.

The aeromagnetic data was obtained from Nigeria Geological Survey Agency (NGSA). The data were captured for NGSA from 2005 to 2010 by Fugro Airborne Surveys as part of nationwide airborne geophysical surveys. The data were acquired along a series of NE–SW profiles with a flight line spacing of 500 m and terrain clearance of 80 m. For this study one half degree sheet covering the study area was utilised. The total magnetic intensity field was IGRF [37] corrected and a super-regional field of 32,000 nT was deducted from the raw data. Oasis montaj software was used to grid the data at 125 m spatial resolution using the minimum curvature gridding method [38] and subsequently subjected to Reduction to the Magnetic Equator (RTE) and further processing were carried out in order to investigate the presence of buried structures that might be relevant in mineral exploration.

2.2. Geological and Structural Mapping

The geological and structural base map used in this research were digitized from the Geological Map of Keffi Sheet 208 on a scale of 1: 100,000. Geological field mapping was done on a scale of 1:25,000 in validating and updating the geological map of the study area. This map was also used as input datasets in remote sensing image interpretations and integration so as to identify major lithologic units in the study area. Also, locations of mineral occurrences were clipped from the Mineral map of Nigeria.

Detailed structural mapping was done in a grid format.

This ensured not less than 80% of the study area was accessed and mapped. 70 locations indicated exposed lithologies either as prominent outcrops or pegmatite intrusions. Others were mapped along stream channels, road cuts or weathered rocks. Artisanal mine pits were also investigated. Fractures were investigated in all the locations. After a careful survey over an outcrop and its surroundings, measurements of the predominant and distinct joint sets were made. Orientations of prominent intrusions were also recorded. Landsat imagery, SRTM elevation and Aeromagnetic data were processed in so as to produce thematic images of First vertical and Tilt derivative maps for geological interpretation. The preliminary interpretations were field validated and new information gathered were used for an updated interpretation. These new interpretations were integrated with other information generated from the datasets, thus allowing the definition of possible target areas of pegmatite hosted mineralizations. The target areas were subsequently ranked according to their mineral potential.

2.3. Data Processing

2.3.1. Structural Data Processing

Data obtained from field structural mapping was used to produce a rose diagram to illustrate principal joint directions.

2.3.2. Landsat Image Processing

Processing of Landsat images included Optimum Index Factor (OIF) calculations (to select the best band combinations) and band ratio calculations. The OIF formula allows the selection of the spectral bands and band ratios for RGB colour composites. The band set with the highest OIF values are the most adequate for RGB colour composites since they combine the largest amount of information (maximum variance) with minimum duplication (low correlation between bands) [39].

2.3.3. Band Rationing

This is a straightforward and powerful remote sensing method that has been widely used in mapping alteration zones and their associated minerals such as iron oxides [40-43]. It enhances the spectral differences between bands and reduces the effects of topography and albedo. Dividing one spectral band by another produces an image that provides relative band intensities. The image enhances the spectral differences between bands [41, 44-45]. Band ratios selected for mineral detection in this study are OLI band ratio 4/2, 6/5, 6/4 and 6/7. B6/B7—the clay ratio is used for distinguishing argillitic and non-argillitic materials; B4/B2—the iron oxide ratio allows the contrast between FeO and non-FeO materials; B6/B5—the ferrous mineral ratio is used to enhance iron-bearing minerals.

2.3.4. SRTM DEM Processing

Shaded relief representations of SRTM DEM using sun elevation angle of 25° and sun illumination directions of Sun illumination directions of 0°, 45°, 90°, 270° and 315°, perpendicular to the prominent lineaments in the region, were selected to enhance the linear features. Lower solar elevations are usually preferred for structural focused studies since they enhance terrain morphology and structural features while higher solar elevations usually favour lithological interpretation as exemplified by [46]. Enhancement of prominent lineaments for the DEM was achieved by varying the sun illumination angles of the SRTM DEM. Hence, different views of the same area yielded somewhat different lineaments especially those orthogonal to the illumination angle

2.3.5. Aeromagnetic Data Processing

Directional and normalized derivatives of the aeromagnetic data were calculated to accentuate near surface structures from which lineaments were identified and delineated. These included shaded relief, first vertical and tilt derivatives maps. Use of first vertical derivative was proposed by [47] to detect edge of shallow features while suppressing the deeper ones.

The tilt derivative method is extensively used in magnetic data processing to delineate structures (both deep as well as shallow). The tilt angle, first introduced by [48], is the ratio of the first vertical derivative to the horizontal gradient and is designated to enhance subtle and prominent features evenly. These maps show delineated lineaments of relatively shallow features important for mineral exploration efforts.

Magnetic lineaments can be related to faults and fractures or lithologic contacts. Several geologic processes may change the magnetic properties of the bedrock depending on prevailing physical and chemical conditions and mineralogy [49]. Hence, faults and fractures may induce a magnetic minimum or maximum. After a series of interpretation, magnetic minima were found to be more representative of structural features capable of hosting pegmatite mineralizations. A composite of all magnetic lineaments and their corresponding rose diagram were constructed.

The Source Parameter Imaging (SPI) method [50] estimates the depth from the local wavenumber of the analytic signal. Source Parameter Imaging algorithm using the MAGMAP extension of oasis Montaj software was applied to the RTE magnetic data to model depth to causative bodies. Depths to causative bodies for every 250 m^2 were estimated.

2.4. Geological Interpretation and Field Validation

The processed digital images resulting from the Landsat 8 imagery and the shaded relief representation maps from SRTM DEM were visually interpreted using geological photointerpretation methods resulting in preliminary lineament maps. Field verification was carried out in order to identify mapped features on the ground, thus verifying their possible geological meaning and to identify possible false positives. Subsequently, lineament reinterpretation followed the fieldwork where the original digital processed images were reinterpreted, resulting in new lineament maps new lineament interpretations were merged, thus resulting into a composite final lineament map.

2.5. Lineament Data Integration

The statistical analyses of the lineaments in the present study were based on the length and total number of the lineaments. The maximum, minimum and average length as well as the standard deviation of the length of the lineaments were also analysed. Rose diagram analyses were generated to show the orientation distribution of the lineaments.

Rockworks 16 (RockWare) software tools were utilized to construct rose diagrams. The final composite lineament map was used to create a lineament density map (in length per unit of area) using the line density function of ArcGIS with a 1 km search radius. Mapped lineaments were compared with data from geologic and surface structural mapping. Mineral occurrences map (including locations of active artisanal and abandoned mine pits) were also analysed.
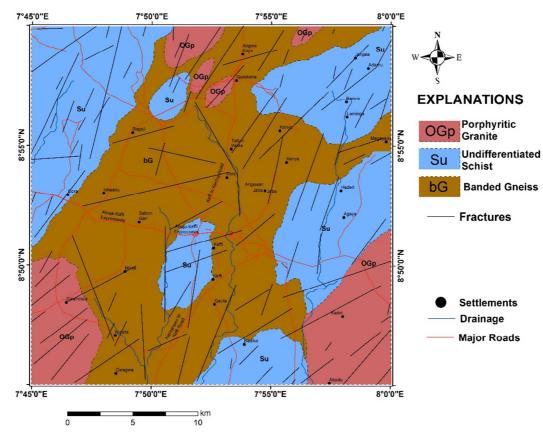
3. Result

3.1. Geology and Surface Structural Mapping

Figure 1. Geologic map of the study area.

3.1.1. Schist

The schists show some observable characteristic variations in composition mostly in either the mica contents or the quartzo – feldspathic contents. Most are micaceous and semi-pelitic to pelitic schists, while others are amphibolites schists that show striation. The schists are fine to medium-grained, strongly foliated rocks and contain numerous porphyroblasts of resistant minerals like garnet and andalusite. There are indications that the schists have undergone a polyphase metamorphism and ductile deformations evidenced by local variations in the strikes and dips of the foliations as measured on the field. Areas underlain by schists are generally low in relief or altitude and form extensive pediplain, except where a pegmatite dome occurs or low-lying hills of gneiss or granites intrusion. They mostly serve as river beds and control the stream flow direction.

3.1.2. Granite

They occur as intrusions (schists were intruded by granite), massive bodies and are extensive. The granites are an-orogenic and they are biotite-granites; they outcrop as hills especially at the north-central and south-eastern part of the study area. These granites have a range of granodiorite to granite compositions and are porphyritic. Their coarse grains are indicative of rate of cooling in relation to the environment. The porphyritic granites contain pink-feldspar, quartz and biotite.

3.1.3. Gneiss

These are granitic rocks with the alignment of biotite minerals i.e. a granite with gneissosity texture they displayed grey foliated biotite and hornblende. They are quartzo-feldspathic rock of granodiorite to quartz diorite composition. Alternating mafic and

quartzo-feldspathic materials define a fine banding. The contacts between the mafic and felsic materials were gradational. Calc-gneiss, amphibolites and dolerite are the types of gneiss that were observed; they intrude the schist and are the dominant rock suite of the entire mapped area, but are more predominant in the central, southwestern and eastern parts where they have distinct and observable boundaries with the schists and granites. In some cases, the gneisses are dissected by streams. The dominant minerals consist of mainly of quartz, feldspar and mica. They are light coloured.

3.1.4. Pegmatites

The pegmatites are coarse grained rocks rich in quartz, feldspar and micas. They intrude the gneisses, older granites and the Schist. Those associated with older granites are cross cutting. Pegmatite veins varying in sizes from only a few centimetres to about 500 m in length and about 30m-60m wide are abundant in the area. From hand specimen obtained from the pegmatites, evidence of mineralization was obvious, black lumps, dark and distinctive grains occupy spaces between the feldspars, and there are instances where tourmaline (greenish hexagonal and elongated shape) is exposed on the rock surface. A graphic intergrowth of feldspar and quartz are also observed in some of the larger pegmatite bodies. Many of these pegmatites are domelike, some are regular tabular bodies with fairly constant strike and dip while others have irregular forms.

Two types of pegmatites were distinguished on the basis of their structural inclination (geomorphology). The first and most abundant type occur as concordant intrusions in areas underlain by schist thus forming near flat lying domes and extensive veins. The second type occurs as steeply dipping to nearly vertical bodies intruding mainly the granite suites. In most cases their contacts with the schist are well defined and are macroscopically sharp while diffuse contacts were observed in the granites and gneiss.

3.2. Satellite Imagery

Based on the calculation of the OIF, band 7-6-5 combination was found the most suitable for geological interpretation (Table 2).

Table 2. *Landsat 8 band combinations with the highest OIF values (Band combination were adapted for Landsat 7 ETM+ band designations).*

Landsat 8 OLI Band Combinations			OIF (%)
B5	B6	B7	68.13
B2	B5	B6	64.44
B4	B5	B6	63.88
B3	B5	B6	63.39
B2	B6	B7	62.66
B4	B6	B7	61.87

3.2.1. Preliminary Lineament Extraction

The processed digital images resulting from the Landsat 8 OLI imagery (RGB colour composites, directional high pass filters over band 6 and the hill-shade relief maps of SRTM DEM were interpreted using geological digital image interpretation techniques. From these initial interpretations, the preliminary lineament maps were obtained.
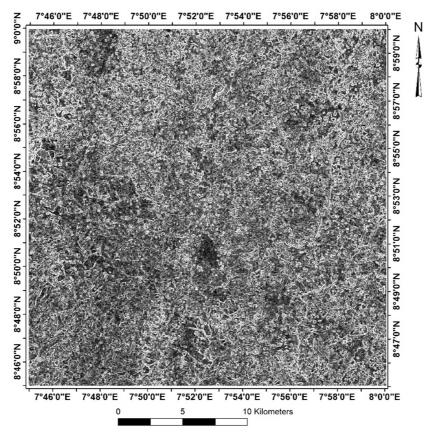

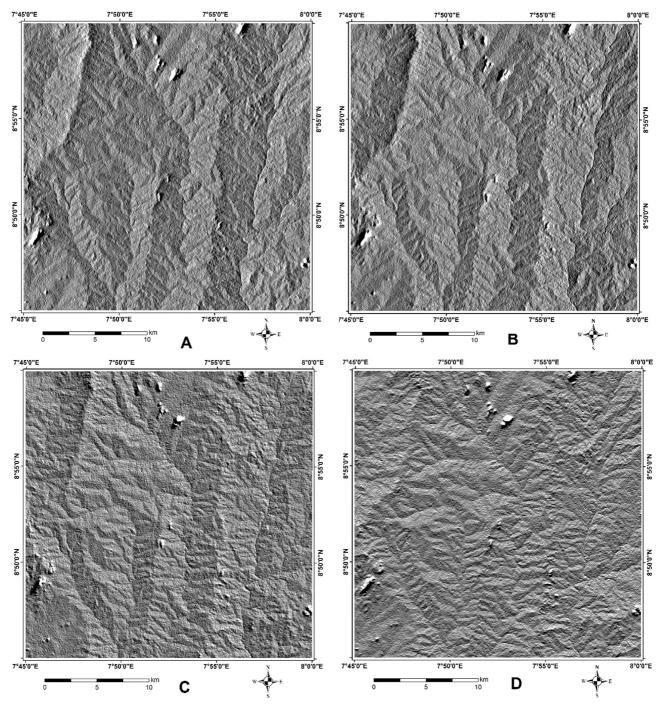**Figure 2.** *Landsat 8 Band 6 Sobel filtered image enhanced for lineament extraction.*

Figure 3. Hill shade relief maps of SRTM DEM: (A) N–S; (B) NE–SW; (C) E–W and (D) NW-SE.

3.2.2. Aeromagnetic Data

Residual magnetic anomaly image (Reduced to Equator (RTE) (Figure 4) shows an amplitude variation in the range of -34 to 34 nT in the study area due to wide variation of susceptibility values of various litho-units (magnetic/moderate-magnetic basement). High amplitude, short wavelength anomaly pattern in the north-eastern part of the area shallow nature of the basement. Since the contact is unconformable, the boundary in magnetic anomaly image is gradational. On contrary, sharp contact is observed in the north-eastern margin because this part marks the boundary between schist and gneiss. The southern part is showing magnetic low as compared to northern part. This indicates that the sediment thickness is probably more in the southern part. The magnetic bodies are oriented in the NE-SW direction marked in the magnetic anomaly image. This is also evident in the hill shade image of the residual magnetic anomaly map (Figure 5).
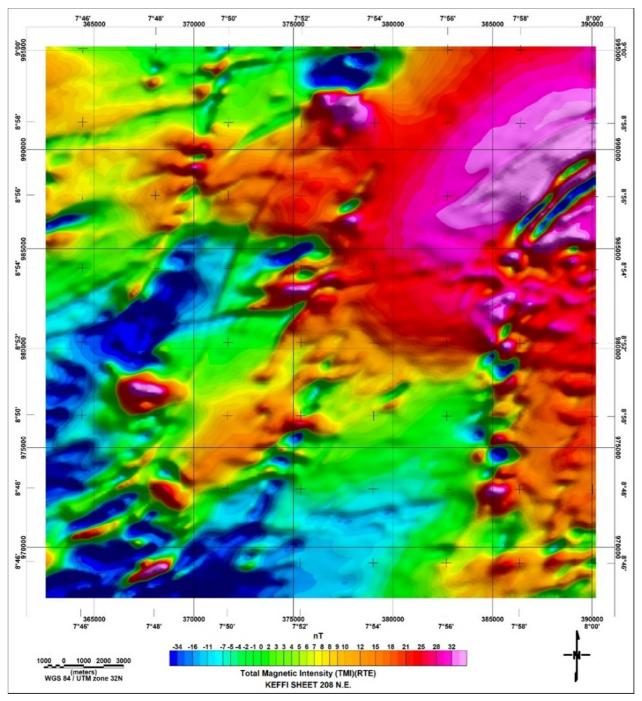
Figure 4. *Residual Intensity Magnetic Anomaly (Reduced to Equator) map.*
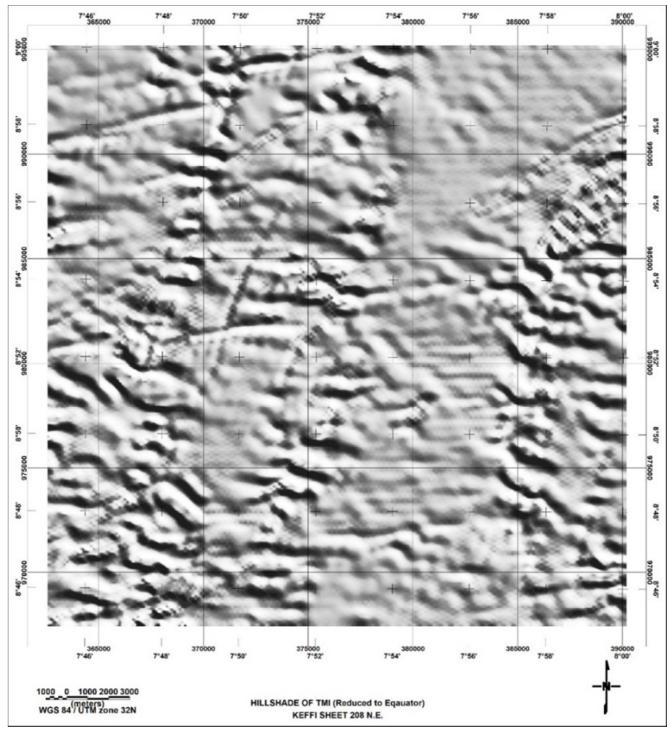
Figure 5. *Hill shade representation of the Residual magnetic anomaly (Reduced to Equator) map.*

Detailed structural fabric has been deciphered based on study of First vertical derivative image (Figure 6) and tilt derivative image (Figure 7). All zones of magnetic minima as well as displacements/discontinuities of magnetic anomalies were interpreted as linear structures. Some of these negative anomalies have remarkable positive anomalies at the edges, though not all of the structures are lined with these positive anomalies. The presence of linear, negative and positive anomalies next to each other is due to the general geometry of magnetic anomalies [51]. First vertical derivative image indicates that magnetic linears generally trend NE-SW sectors with minor NE-SW and E-W components. Linears along NE-SW directions are dominant with minor E-W and NW-SE components. Here, the basement faults (NE-SW) are better resolved.
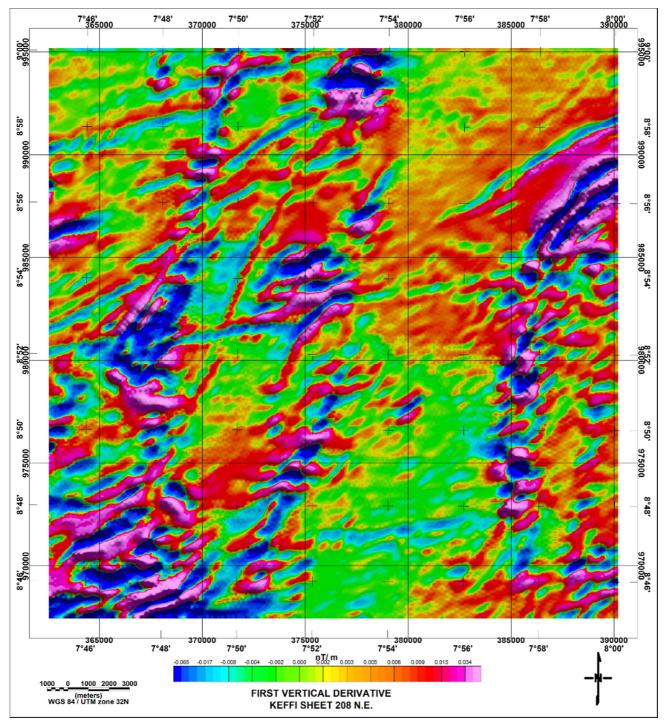
Figure 6. *First Vertical Derivative image of Keffi Sheet 208 NE.*
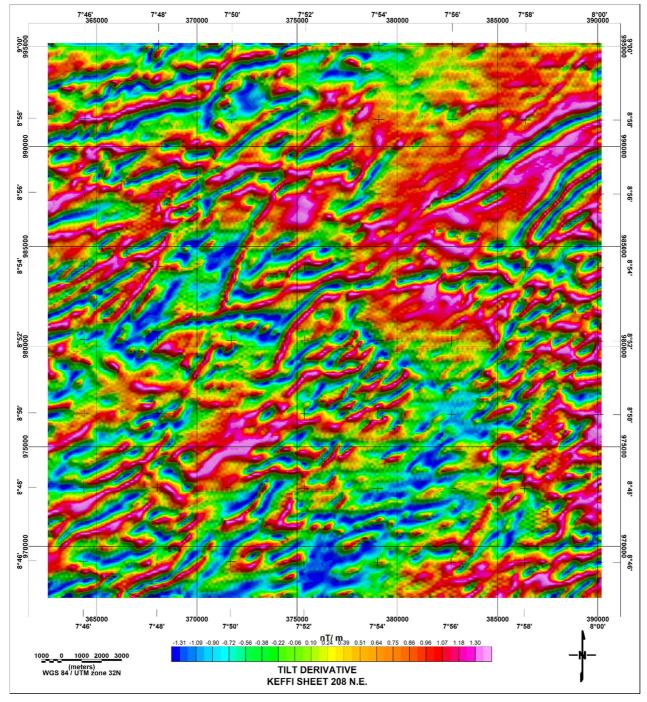
Figure 7. *Tilt Derivative image of Keffi Sheet 208 NE.*

Depth estimation of causative bodies using the SPI method (Figure 8) range from 90 to 600 m. Interestingly, most lineaments were delineated from the study area are coincident in areas of shallow depth especially in the north-eastern portion of the map. This gives much credence to the fact that these sites could be exploited for development of mineral resources.
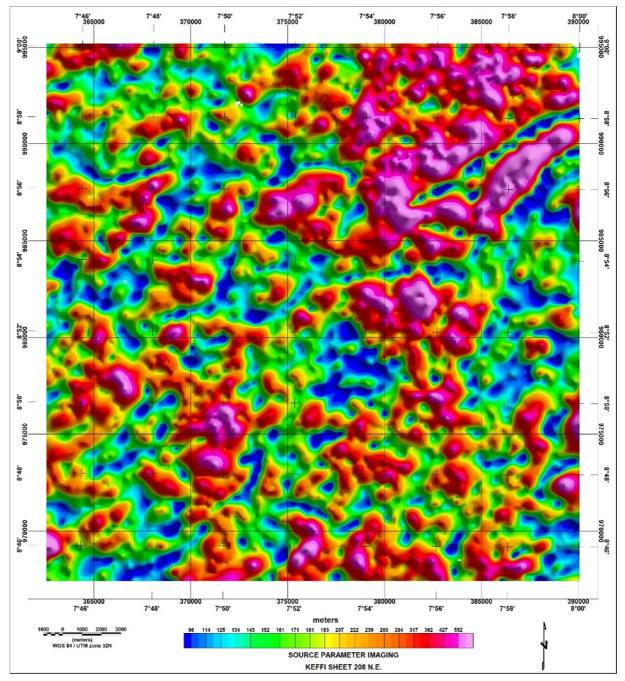
Figure 8. *Source Parameter Imaging (SPI) of Keffi Sheet 208 NE.*

3.3. Field Validation and Lineament Reinterpretation

Field campaign was instituted to authenticate on ground, the results of image processing and interpretation of the lineaments. The campaign focused on structural and geomorphological analysis in a part of the study area. A number of false lineaments were detected from the combined lineament extracted from Landsat 8 and SRTM DEM data. These were attributable to long narrow unpaved roads and some ferruginous clay deposits in the area. Some of the mapped lineaments were identified as real geological features. The resultant final lineament composite map took into account these false lineaments as they were deleted and

while leaving out some probable lineaments that could not be satisfactorily confirmed.

The adjusted surface lineament trends are represented in rose diagram (Figure 9). This shows that the NW–SE trends are the most predominant. This is the trend displayed by many surface fractures resulting from recent geologic events and surface processes. This trend is parallel to the trend exhibited by the younger cretaceous Bida Basin [52, 53]. The predominant NE-SW trend displayed by the magnetic lineaments (Figure 10) suggest tectonic activities that formed the Ifewara – Zungeru transcurrent fault line in which the schist belts where major mineral deposits have been identified in Nigeria [54-56]. Magnetic lineament trends are

depicted in the rosetted diagram (Figure 10). It represents lineaments extracted from the datasets already discussed in previous sections.
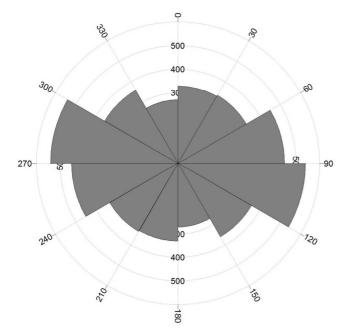

Figure 9. *Rosette diagram of lineaments derived from Landsat 8 and SRTM DEM. Major trend is in the NW-SE direction parallel to the Cretaceous Bida Basin.*

Both surface lineaments and magnetic lineaments were combined to form the composite lineament map of Keffi Sheet 208 NE (Figure 11) and the composite lineament density map was subsequently created and the map values shown in Figure 12. The highest lineament density values (> 6 km/km^2) are found in the north-eastern portion of the study area. High-density lineament values also appear in the southern portion of area.
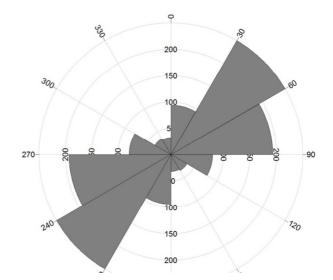

Figure 10. *Rosette diagram of lineaments derived from Hill shade, First Vertical Derivative and Tilt derivative residual magnetic anomaly maps. Principal trend is in the NW-SE direction parallel to the Cretaceous Bida Basin.*
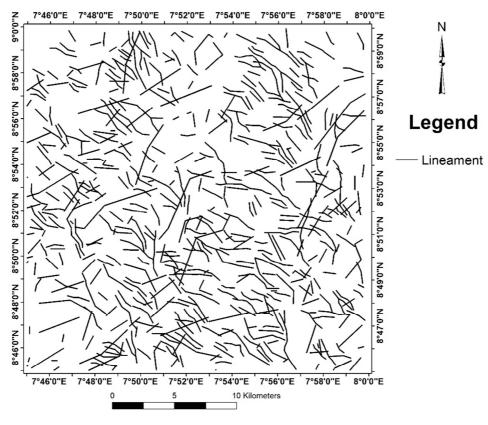

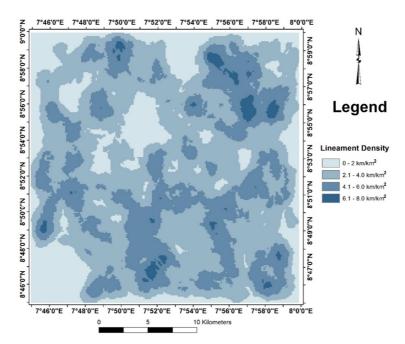***Figure 11.*** *Composite lineament map of Keffi Sheet 208 NE.*

Figure 12. *Lineament density map of Keffi Sheet 208 NE.*

3.4. Band Ratio

The detection of alteration zones marked by the presence of iron oxides, hydroxyl- bearing minerals and hydrothermal clays is possible from false colour composite image band ratios of 6/4, 4/2 and 6/7 in red, green and blue [41, 26, 57-59]. Primary colours of red, green and blue are indicative of high ratio value band ratios of 6/4, 4/2 and 6/7 respectively. High band ratio values of two colours are depicted in the pixel as a combination of two colours proportional to their values. High 6/4 values (red) give a high composition of iron oxides (both ferric and ferrous); large 4/2 values (green) represent a large component of ferric oxides associated soils. Furthermore, high 6/7 values (blue) represent the presence of hydrothermal clays since the band 6 covers the reflectance peak of hydrothermal clays whereas band 7 contains a reflectance trough of the clays. A large 6/4 and 4/2 band ratio values in the same pixel will display as yellow, while high band ratios of 6/4 and 6/7 value in one pixel will be displayed as pink. The largely green areas in the north-eastern portion pf the band ratio composite map correlates well with areas having high lineament densities. These are areas are rich in ferric minerals and hydrothermally altered clays (Figure 13).
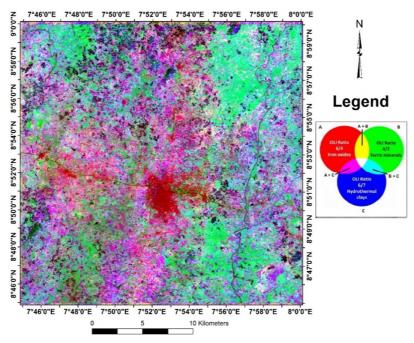

Figure 13. *Composite Band Ratio image of Keffi Sheet 208 NE.*

4. Discussion

The schists have a general strike of north-south, and in the area, dip at angles ranging from 30° to 60° to the east and of much lesser values to the west. There are veins of various lengths and width with dykes and veins of quartz porphyry, quartzo-feldsphatic vein and even pegmatites. The foliation of biotite minerals could be as a result of metamorphism, late intrusion of pegmatite or tectonic activities. The pegmatites are always closely associated with quartz veins more in the gneiss rock suites. Structural features in the area are the penetrative tectonic foliations trending mainly in the N-S, E-W, NE-SW and NW-SE directions, veins, dykes, folding, faults and joints mostly believed to have been reactivated or formed during the Pan African tectonic events (600±150 Ma) [60].

Result of Landsat 8 OLI composite band ratio presented in figure 13, indicates a possible presence of altered and weathered ferric iron oxides in the top soil at the study area. In addition, the composite band ratio result also implies iron oxides are associated with hydrothermally altered rocks. This may mean that altered iron oxides and hydrothermal alteration appear at the surface of the study site.

The geological significance of a lineament may be estimated from the relation of the lineament to other magnetic patterns: Features crosscutting the magnetic anomalies are supposed to be younger than the magnetic sources and predominantly brittle in character, whereas concordant features are supposed to be more ductile. However, the geological observations from the Keffi area show that due to the complex deformation history of the bedrock, the classification of the lineaments using this method may be ambiguous: Many of the old ductile zones have been repeatedly reactivated, showing a semi-brittle and/or brittle character within the same zone.

The comparison of the lineaments and direct geological observation suggests that from the different data sets, magnetic lineaments most likely represent brittle deformation zones. High lineament densities maybe attributable to areas showing great promise for rich mineral deposits. As is shown in the surface interpretation, the presence of hydrothermal alteration and the altered iron oxides on the surface of the study area indicates that iron oxides may exist below surface to be a main magnetic source of the observed positive aeromagnetic anomaly. However, the potential association between lineaments, geology and other attributes can only be positively confirmed with the integration of ground-based geophysical and geochemical datasets.

5. Conclusion

The application of digital image processing algorithms to Landsat 8 scene and SRTM DEM produced surface lineaments using geological photointerpretation techniques. Aeromagnetic data was also processed using standard image analysis and derivative maps were produced from which magnetic lineaments were extracted. These were subsequently integrated and after diligent fieldwork campaign validation, new geological–structural elements were identified and added to the map while false lineaments were deleted from the final lineament map. The integration of remote sensing data with information from the aeromagnetic data led to the identification of probable locations pegmatite hosted mineral occurrences.

More detailed work would entail integrating these datasets with radiometric data and other ground-based geophysical and geochemical datasets to constrain information from the present work. Places that have recorded mineral occurrences needs to be mapped in detail.

References

[1] Matheis, G. (1987). Nigerian rare-metal pegmatites and their lithological framework. Geological Journal, Vol. 22, Thematic Issue, 271-291.

[2] Garba, I., (2003). Geochemical Discrimination of Newly discovered rare-metal bearing and barren pegmatites in the Pan-African (600±150 Ma) basement of northern Nigeria. *Applied Earth Science* (Trans. Inst. Min. Metall.), vol. 112.

[3] Olugbenga A., Okunlola O. A. and Ocan O. O. (2009). Rare metal (Ta-Sn-Li-Be) distribution in Precambrian pegmatites of Keffi area, Central Nigeria. *Nature and Science*. 7 (7). ISSN 1545-0740. http://www.sciencepub.net

[4] Tanko, I., Adam, M., Dambring, P. (2015). Field features and mode of emplacement of pegmatites of Keffi area, north central Nigeria. *Int. J. Sci. Technol. Res*. Volume 4, Pages 214-229.

[5] Obaje, N. G. (2009). *Geology and Mineral Resources of Nigeria*: Germany: Springer Publishers.

[6] Oyinloye, A. O. (2011). Geology and geotectonic setting of the basement complex rocks in South Western Nigeria: implications on provenance and evolution. In Earth and Environmental Sciences. InTech.

[7] Kayode, J. S., Nawawi, M. N. M., Abdullah, K. B., & Khalil, A. E. (2017). Integrating aeromagnetic and Landsat™ 8 data into subsurface structural mapping of Precambrian basement complex. *Journal of African Earth Sciences*, *125*, 202-213.

[8] Aliyu, A. S., Musa, Y., Liman, M. S., Abba, H. T., Chaanda, M. S., Ngene, N. C., & Garba, N. N. (2018). Determination of rare earth elements concentration at different depth profile of Precambrian pegmatites using instrumental neutron activation analysis. Applied Radiation and Isotopes, 131, 36-40.

[9] Akande, S. O. and Reynolds, P. H. (1990). ^{40}Ar/ ^{39}Ar spectrum ages of micas from the Sn-Nb-Ta bearing pegmatites in Nigeria. In: Proceeding, Volume 15, Colloquium of African Geology. Centre International Pour la Formation Et les Echanges Geologiques (CIFEG) Occassional Publication 1990/20 p243.

[10] Dada, S. S., Lancelot, J. R. and Briqueu, I. (1987). Age and origin of a Pan-African charnockitic complex: U-Pb and Rb-Sr evidence from the charnockitic complex at Toro, Northern Nigeria. Abtr. Vol. 14 Coll. Afri. Geol. Berlin, 72-73.

[11] Umeji, A. C. and Caen-Vachette, M. (1984) Geochronology of Pan-Africa Nasarawa Eggon and Mkar Gboko granites, South East Nigeria. *Precambr. Res*. 23, 317-324.

[12] Matheis, G. and Caen-Vachette, M. (1983). Rb-Sr isotopic study of rare-metal bearing and barren pegmatites in the Pan-African reactivation zone of Nigeria. *J. Afr. Ear. Sci*. 1, 35-40.

[13] Rahaman, M. A., Emofurieta, W. D., Caen-Vachette, M. (1983). The potassic granites of the Igbeti area: Further evidence of the polycyclic evolution of the Pan-African belt in South-Western Nigeria. *Precamb. Res*. 22, 27-92.

[14] Olisa, O. G., Okunlola, O. A., & Omitogun, A. A. (2018). Rare Metals (Ta-Nb-Sn) Mineralization Potential of Pegmatites of Igangan Area, Southwestern Nigeria. Journal of Geoscience and Environment Protection, 6 (04), 67.

[15] Ball, E. (1980). An example of very consistent brittle deformation over a wide intracontinental area: the late Pan-African fracture system of Tuareg and Nigerian shield. Tectonophysics, 61: 363-379.

[16] Holt, R., Egbuniwe, I. G., Fitches, W. R. and Wright, J. B. (1978). The relationship between low-grade metasedimentary belts, Calc-alkaline volcanism and the Pan-African Orogeny in NW Nigeria. *Geol. Rundsch*, 67, pp- 631-646.

[17] Awoyemi, M. O., Hammed, O. S., Falade, S. C., Arogundade, A. B., Ajama, O. D., Iwalehin, P. O., & Olurin, O. T. (2017). Geophysical investigation of the possible extension of Ifewara fault zone beyond Ilesa area, southwestern Nigeria. Arabian Journal of Geosciences, 10 (2), 27.

[18] McCurry, P. (1973). Geology of degree Sheet 21 (Zaria). *Overseas Geology and Mineral Res*ources, 45 HMSO, London.

[19] Ajibade, A. C. (1989). Provisional Classification of the Schist Belts of North-Western Nigeria. In Kogbe, C. A. (Eds.), *Geology of Nigeria (*pp. 85-90). Rockview International, Jos.

[20] Kuster, D. (1990). Rare-metal pegmatites of Wamba, Central Nigeria-their formation in relationship to late Pan-African granites. Mineralium Deposita 25, 25-33.

[21] Garba, I. (1992). Geology, geochemistry and origin of gold mineralization at Bin Yauri, Nigeria. PhD Thesis, University of London, UK. pp 264.

[22] Ekwueme, B. N. and Matheis, G. (1995). Geochemistry and economic value of pegmatites in the Precambrian basement of Southeast Nigeria. In: Magmatism in relation to diverse tectonic settings (Eds. R. K. Srivastava and R. Chandra), 375-392p. New Delhi, Oxford & IBH Publishing Co.

[23] Garba, I. (2002). Late Pan-African Tectonics and origin of Gold Mineralisation Rare-Metal Pegmatites in the Kushaka Schist Belt, North-Western Nigeria. Journ. of in. and Geol. 38 (1) 2002, 1-12.

[24] Gupta, R. P. (2017). Remote sensing geology. Springer.

[25] O'Leary, D. W., Friedman, J. D. & Pohn, H. A. (1976). Lineament, linear, lineation: Some proposed new standards for old terms. *Geological Society of America Bulletin*, 87, 1463–1469.

[26] Knepper, D. H., Jr., (1989). Mapping hydrothermal alteration with Landsat Thematic Mapper data, Lee, Keenan, ed., Remote sensing in exploration geology — A combined short course and field trip: 28th International Geological Congress Guidebook T182, p. 13–21.

[27] Cudahy, T. J., Caccetta, M., Thomas, M., Hewson, R. D., Abrams, M., Kato, M.,... Mitchell, R. (2016). Satellite-derived mineral mapping and monitoring of weathering, deposition and erosion. Scientific reports, 6, [23702]. doi: 10.1038/srep23702.

[28] Madani, A. A (2009). Utilization of Landsat ETM+ Data for Mapping Gossans and Iron Rich Zones Exposed at Bahrah Area, Western Arabian Shield, Saudi Arabia. *JKAU: Earth Sci*., Vol. 20 No. 1, pp: 35-49.

[29] Singer, R. B. (1981). Near-infrared spectral reflectance of mineral mixtures – systematic combinations of pyroxenes, olivine, and iron oxides, J. Geophys. Res., 86, 7967–7982. doi: 10.1029/JB086iB09p07967.

[30] Hunt, G. R. (2017). Spectroscopic properties of rocks and minerals. In Handbook of Physical Properties of Rocks (1982) (pp. 295-386). CRC Press.

[31] Blakely, R. J. (1995). Potential Theory in Gravity and Magnetic Applications. Brooklyn, NY: *Cambridge University Press*.

[32] Watkins, D. (2018). *30-Meter SRTM Tile Downloader*. Retrieved from: http://dwtkns.com/srtm30m/.

[33] Reuter, M., Buchwitz, M., Hilker, M., Heymann, J., Schneising, O., Pillai, D.… (2014). Satellite-inferred European carbon sink larger than expected. *Atmos. Chem. Phys*., 14, 13739-13753. https://doi.org/10.5194/acp- 14-13739-2014.

[34] USGS/NASA (2015). Landsat 8 (L8) Data User's Handbook; USGS/NASA: Sioux Falls, SD, USA, p. 106.

[35] U.S. Geological Survey. (2018). *EarthExplorer*. Retrieved from: https://earthexplorer.usgs.gov

[36] Reynolds, R. L., Rosenbaum, J. G., Hudson, M. H., & Fishman, N. S. (1990). Rock magnetism, the distribution of magnetic minerals in the Earth's crust, and aeromagnetic anomalies, in Hanna, W. F., ed., Geologic applications of modern aeromagnetic surveys: U.S. Geological Survey Bulletin 1924, p. 24–45.

[37] International Geomagnetic Reference Field - 11th Generation (2009). https://www.ngdc.noaa.gov/metaview/page?xml=NOAA/NES DIS/NGDC/MGG/GeophysicalModels/iso/xml/IGRF11.xml& view=getDataView&header=none.

[38] Briggs, I. C. (1974). Machine contouring using minimum curvature. *Geophysics*, *39* (1), 39-48.

[39] ITC (2007). Integrated Land and Water Information System (ILWIS). ILWIS 3.31 Academic. University of Twente, Netherlands.

[40] Li, M. (2017). Aeromagnetic and Spectral Expressions of Rare Earth Element Deposits in Gallinas Mountains Area, Central New Mexico, USA.

[41] Sabins, F. (1997). Remote Sensing: Principles and interpretation (2nd ed.). NY: Freeman.

[42] Shalaby, M. H., Bishta, A. Z., Roz, M. E., & El Zalaky, M. A. (2010). Integration of geologic and Remote Sensing Studies for the Discovery of Uranium Mineralization in Some Granite Plutons, Eastern Desert, Egypt. Journal of King Abdulaziz University: *Earth Sciences*, 21 (1).

[43] Dehnavi, A. G., Sarikhani, R., & Nagaraju, D. (2010). Image processing and analysis of mapping alteration zones in environmental research, East of Kurdistan, Iran. *World Applied Sciences Journal*, 11, 278–283.

[44] Howari, F. M., Baghdady, A. and Goodell, P.C. (2007). Mineralogical and geomorphological characterization of sand dunes in the eastern part of United Arab Emirates using orbital remote sensing integrated with field investigations. Geomorphology, 83, pp. 67-81.

[45] Exelis Visual Information Solutions (2012). ENVI Classic Help. Boulder, Colorado: Exelis Visual Information Solutions.

[46] Rabaça, T., Vicente, A. M. P. & Pereira, A. J. S. C. (2006). Appliance of spectral data from the optical and microwave data to the geological mapping of central Portugal: preliminary data (in Portuguese). Proceedings of the VII National Congress of Geology, III, University of Évora, pp. 1119-1122.

[47] Nabighian, M. N. (1984). Toward a three-dimensional automatic interpretation of potential field data via generalized Hilbert transform: Fundamental relations. *Geophysics,* 47, 780-786.

[48] Miller, H. G. and Singh, V. (1994). Potential-field tilt - a new concept for location of potential-field sources. Journal of Applied Geophysics, v. 32, p. 213-217.

[49] Airo, M. L. (2005). Regional interpretation of aerogeophysical data: Extracting compositional and structural features. In Airo, M. L. (Eds.), *Aerogeophysics in Finland 1972–2004: Methods, System Characteristics and Applications.* Geological Survey of Finland, Special Paper 39, 21–74.

[50] Thurston, J. B., & Smith, R. S. (1997). Automatic conversion of magnetic data to depth, dip, susceptibility contrast using the SPI^{TM} method. Geophysics, 62, 807–813.

[51] Telford W. M., Geldart, L. P. & Sheriff, R. E. (1990). Applied geophysics, Cambridge University Press.

[52] Oluyide, P. O. (1988). Structural trends in the Nigerian Basement Complex. In: Precambrian Geology of Nigeria. *Geological Survey of Nigeria*, pp. 93-98.

[53] Megwara, J. U. & Udensi, E. E. (2014). Structural Analysis Using Aeromagnetic Data: Case Study of Parts of Southern Bida Basin, Nigeria and the Surrounding Basement Rocks. *Earth Science Research*, 3 (2), 27-35.

[54] Ojo, S. B. (1990). Origin of a major aeromagnetic anomaly in the Middle Niger Basin, Nigeria. *Tectonophysics*, 185 (1), 153-162.

[55] Olasehinde, P. I., Pal, P. C. & Annor, A. E. (1990). Aeromagnetic anomalies and structural Lineaments in the Nigerian Basement Complex. Journal of African Earth Sciences, 1 (3&4), 351-355.

[56] Nwankwo, L. I., Olasehinde, P. I., & Sunday, A. J. (2018). Fractal Revaluation of Bottom Depth of Magnetic Sources in Bida Basin, Nigeria from High-Resolution Aeromagnetic Data. J. Ind. Geophys. Union (March 2018), 22 (2), 143-150.

[57] Khalid A., Elsayed Z. & AbdelHalim H. (2014). The Use of Landsat 8 OLI Image for the Delineation of Gossanic Ridges in the Red Sea Hills of NE Sudan. *American Journal of Earth Sciences*. Vol. 1, No. 3. pp. 62-67.

[58] Pour, A. B., Hashim, M. & Marghany, M. (2014). Exploration of gold mineralization in a tropical region using Earth Observing-1 (EO1) and JERS-1 SAR data: a case study from Bau gold field, Sarawak, Malaysia. Arab J Geosci 7: 2393. https://doi.org/10.1007/s12517-013-0969-3.

[59] Ducart, D. F., Silva, A. M., Toledo, C. L. B., & deAssis, L. M., 2016. Mapeamento de óxidos de ferro usando imagens Landsat-8/OLI e EO-1/Hyperion nos depósitos ferríferos da Serra Norte, Província Mineral de Carajás, Brasil. Brazilian Journal of Geology. 46, 331-349.

[60] Dada, S. S. (2006). Proterozoic evolution of Nigeria. In Oshi O. (Eds.), The Basement Complex of Nigeria and its Mineral Resources (A tribute to Prof. M. A. Rahaman). (pp. 29-44). Akin Jinad and Co. Ibadan.